

Contribution of the Image-Assisted Theodolite System QDaedalus to Geodetic Static and Dynamic Deformation Monitoring

S. Guillaume, J. Clerc

Institute of Geodesy and Photogrammetry, ETH Zurich, Switzerland

C. Leyder

Institute of Structural Engineering, ETH Zurich, Switzerland

J. Ray, M. Kistler

Federal Office of Topography, swisstopo, Wabern, Switzerland

Abstract. QDaedalus is an image-assisted theodolite based system devised at the Institute of Geodesy and Photogrammetry at ETH Zurich where both, hardware and software development were carried out. The basic idea is to replace the eye-piece of an existing total station by a CCD camera in a non-destructive way in order to measure fully automatically and very accurately spatial directions to visible objects without using corner-cube targets as in standard Automatic Object Recognition (ATR). Small electronic interfaces for indoor and outdoor hardware synchronization of several QDaedalus systems allowing for contactless measurements of several deforming and oscillating objects at very high precision (~ 0.01 mm) at high sampling rate (60 Hz) in three dimensions.

The system QDaedalus is presented by two experiments conducted at ETH Zurich in the frame of static and dynamic structure monitoring. The first (static) consisted of carrying out, fully automatically angular measurements series on target fixed on a dam, and to evaluate the performance in terms of precision and rapidity of QDaedalus with respect to manual observations. In the second (dynamic) experiment the precise response of a wooden frame subjected to various forcing has been determined. The structure was monitored by accelerometers and on two points by QDaedalus. The two points separated by 12 meters were synchronously measured by 4 theodolite systems revealing the three dimensional point's position.

Keywords. Image-Assisted Theodolite, Geodetic Deformation Monitoring, Dynamic Structure Monitoring, 3D Positioning

1 Introduction

In this paper, we want to present the large spectrum of applications conceivable by the image-assisted theodolite system QDaedalus for deformation monitoring. After a brief description of the system, two experiments are presented. The first consists in measuring targets on a dam in an automated manner, the second shows the potential of measuring high dynamic movements of a structure in 3D with high precision.

2 QDaedalus System Description

The system QDaedalus consists of hardware and software components.

2.1 Total Station

The main sensor is a motorized Leica total station. The compatibility is ensured for the following models: TCA, TPS, TS and MS. However, it is preferred to use a model of the last generation which provides a digital automation of the focus.

2.2 CCD Camera

The basic idea is to remove the existing eyepiece and plug a modified industrial CCD camera in a non-destructive and easy way (Figure 1).

The CCD camera is a modified Guppy F-080C from Allied Vision Technologies (AVT). It is a monochrome camera with 1024x768 pixels, an electronic trigger, and a global shutter providing up to 30 full frames per seconds, or 60 frames per seconds with a reduced field of view. This gives an angular resolution of 4 arcsec (1.1 mgon) per pixel and a field of view of approximately 1 degree.

The main advantages of using our dedicated CCD camera instead of using the existing internal coaxial camera available in the last generation of total stations are the following:

- We can use total stations which are not equipped with an internal coaxial camera.
- We can benefit of the global shutter and the electronic triggering for applications where the timing and the synchronization are an issue.
- The high speed interface permits high-rate real-time applications.



Fig. 1 CCD camera plugged on a TDA5005 (left), TS15 (middle), MS50 (right).

2.3 Divergent Lens

Since the images must be formed in the plane of the CCD chip instead of the plane of the reticulum, sharp image are only possible for objects up to 13 meters. For this reason, a slightly divergent lens can be plugged directly on the objective of the total station permitting a sharp image acquisition from 1.5 meters to infinity.



Fig. 2 Divergent lens plugged on the objective.

2.4 Focusing Mechanism

In order to be able to obtain sharp images without human intervention at any ranges, it is necessary to

have a focus mechanism controllable in a remote way. In the last generation of total station, as the MS or TS models equipped with a coaxial camera, this is already available and the focus can be easily steered via the existing interface.

For the previous generation of total stations a non-destructive focus mechanism based on a stepper motor with a conic gearwheel and a tooth belt was successfully developed by Knoblach (2009), see Figure 1 (left).

2.5 Synchronization Device

In order to take benefit of the electronic triggering of the CCD camera, a synchronization device was designed (Figure 3). It generates synchronized TTL pulses for outdoor as well as for indoor applications. For outdoor applications, the synchronization is easily obtained by an ublox low-cost GNSS receivers. For indoor purposes, a device (configured as master) generates and sends the pulses to the other devices (configured as slaves) via wires or via a wireless transmission. In this case, the distances between the master and the slave devices must not exceed 100 meters.

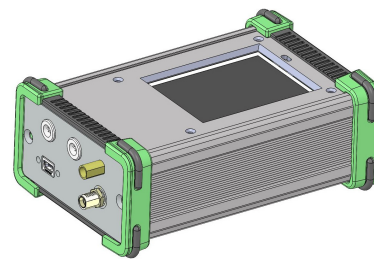


Fig. 3 Synchronization device.

2.6 Software

A user-friendly software specially dedicated for automated image-assisted measurements was completely developed in our Institute. It is permanently improved and adapted to new applications.

3 Automated Static Angular Measurements on a Dam

Up to now, the system QDaedalus was successfully deployed for automated static angular measurements in indoor micro-triangulation applications. In Guillaume et al. (2012), it is shown that the 3D positions of ceramic spheres, placed on particle

accelerator modules (1x4x1 meters), can be remotely and automatically measured by a micro-triangulation network, with a precision better than 10 microns.

In this paper, we want to illustrate the capability of the image-assisted system QDaedalus for a typical outdoor geodetic application: precise angular measurements in the context of the monitoring of dams by geodetic networks.

Nowadays, this task is usually performed in a mixed way. On the one hand, if benchmarks can be equipped with reflector prisms, the measurements are carried out using automatic target recognition (ATR). On the other hand, when benchmarks are simply materialized by optical targets, they are carried out manually by a human operator. The optical targets were commonly in use for old facilities but even so chosen in for the establishment of modern networks for points of which the circumstances are not suited for the installation of prisms (humidity, price, etc...).

Comparing to indoor measurements, outdoor image-assisted measurements are more challenging. The main reason is that the lighting conditions are not controllable and the images are subjected to rapid and unavoidable variations of the luminosity and contrast. Seconds while the targets are usually further distant as for indoor networks. The scintillation due to atmospheric turbulences can generate significant blurring and distortions, making the automatic identification and extraction of targets more fastidious.

In this context, we decided to update and improve the existing algorithm implemented in QDaedalus in order to automate the angular measurements on standard non prismatic targets, used by the Federal Office of Topography swisstopo, on dams (Clerc, 2015).



Fig. 4 Standard swisstopo target for dams.

The standard swisstopo target (Figure 4) is formed by three concentric circles of 22 and 12 and 5 mm, respectively. Their projections in the CCD plane are ellipses for the general case. The sizes in the image of the different circles at different distances are given in Table 1.

Table 1. Size of the different circles in the object space and the image space at different distances.

Distance to target [m]	Target's size [mm]	Size in image [pixel]
10	22	113
	12	62
	5	26
150	22	8
	12	4
	5	1

At large distances, the size of the circles are less than 10 pixels and the identification of all ellipses are very challenging. This requires several image and data processing steps which are described in the following section.

3.1 Multi-ellipses Matching

The aim was to develop an algorithm which allows the identification and the extraction of the parameters of the concentric ellipses in a robust way, with a sub-pixel accuracy, and with a number of input parameters as limited as possible. The algorithm takes as input a single image and a region of interest (ROI). The output is formed by the center of the ellipses and its empirical standard deviation; the parameters of the extracted ellipses (the semi-major axis, the semi-minor axes with their orientation angles).

The processing can be divided in the following steps (Figure 5):

- 1) Image filtering and contrast enhancement. It consists in applying a standard Gaussian filtering of 3x3 pixels and a linear contrast stretching of the histogram according to Luhmann (2014).
- 2) Multiple Otsu thresholding according to Liao et al. (2001). Here, the compromise between the sensitivity and the computation time lead to segment only 3 classes. The output is a binary image.

- 3) Rejection of blobs. White regions with areas smaller than 10 pixels and white regions touching the ROI are rejected.
- 4) Extraction of edges according to Canny (1986).
- 5) Rejection of linear segments. The linear segment are detected by a Hough Line transform.
- 6) Classification of edges in distinct objects. The pixels which fulfill the neighboring condition with a gap tolerance of 3x3 pixels are assumed belonging to the same object.
- 7) Robust ellipse fitting. For each object (if # pixels > 10), a robust ellipse fitting is performed. The adjustment is performed according to Fitzgibbon (1995) with an iterative 3-sigma rejection criteria.
- 8) Robust determination of the center of the ellipses. Once the ellipses are fitted, the final center is given by a robust mean value, with a 3-sigma rejection criteria.

3.2 Precision of the Multi-ellipses Algorithm in Laboratory Conditions

The precision of the multi-ellipses algorithm was tested in the laboratory by measuring and extracting the centers of targets of different sizes (to simulate the apparent size from 10 to 320 meters) located at a distance of 10 meters (to mitigate the effect of scintillation). For each target, 500 shots were carried out and the standard deviations computed of the time series formed are given in Table 2. In these laboratory conditions, the values represent the ultimate precision which can be attained (for one image) with the multi-ellipses algorithm. Up to a distance of 160 meters, they are below to 0.06 pixel corresponding to 0.24 arcsec (0.07 mgon).

Table 2. Standard deviation of multi-ellipses extraction algorithm for targets at different apparent distances.

Apparent Dist. [m]	Std. dev. vert. [pixel]	Std. dev. hz [pixel]
10	0.03	0.05
40	0.03	0.03
80	0.06	0.06
160	0.04	0.06
320	failed	failed

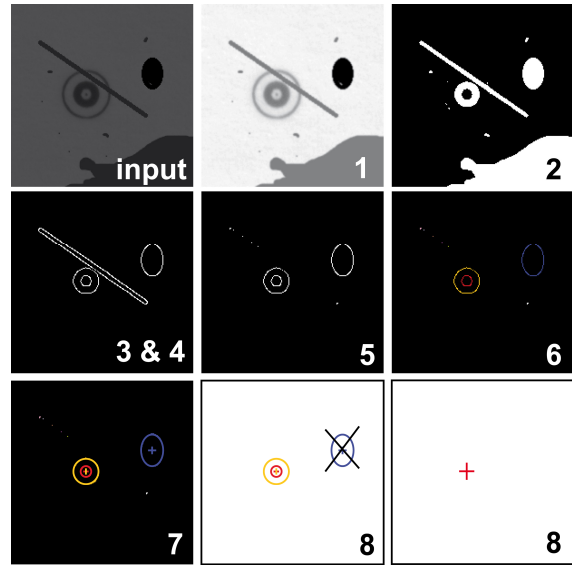


Fig. 5 Processing steps of the multi-ellipses matching algorithm.

3.3 Precision of the Angular Measurements in Laboratory Conditions

In a second validation step, the whole angular measurement process was evaluated in term of precision by performing 10 sets of angular measurements on 7 targets at different locations in the laboratory (Figure 6). The total station Leica MS50 was used. According to the specifications, the angular nominal accuracy is given at 1 arcsec (0.3 mgon).

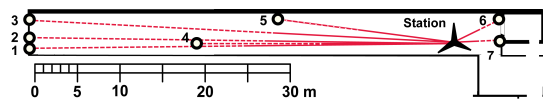


Fig. 6 Positions of the station and the targets in the laboratory.

A set of angular measurements consists of a single QDaedalus angular measurement on each target in the two positions of the telescope. A single QDaedalus angular measurement in one position of the telescope consists of 2 readouts of the theodolite and 20 CCD shots. The first theodolite's readout is combined with a robust mean value of the first 10 extracted centers. The second readout is combined with the last 10 shots. The two angular values are averaged and provide a single QDaedalus angular measurements in one position of the telescope.

A summary of the results is given in Table 3. It shows that the precision obtained in laboratory

conditions is almost one order of magnitude better than the angular accuracy given in the specification of the MS50.

Table 3. Summary of the angular measurements in laboratory conditions.

Results	Zenith angles	Hz directions
# targets	7	7
# sets	10	10
Std dev. of 1 set	0.2 arcsec	0.1 arcsec

3.4 Precision of the Angular Measurements in Field Conditions (Dam)

In order to test and validate QDaedalus in real field conditions, some measurements were carried out on optical targets fixed on a dam monitored by swisstopo. The aim was to compare, in terms of precision and rapidity, the full QDaedalus automatic process (QD) with the standard semi-automatic process in common use at swisstopo (STopo). The experiment consisted in carrying out, from the same pillar, some sets of angular measurements on 18 targets fixed on the dam. The QDaedalus system was installed on a total station Leica MS50 (1 arcsec, 0.3 mgon) while the team of swisstopo used a total station Leica TDA5005 (0.5 arcsec, 0.15 mgon). The sets were carried out alternatively by the two systems. The internal precisions obtained by QD and STopo are given in Table 4 and 5. As we can see, the internal precision of QD is more than 2 times better than the internal precision of STopo. Concerning the rapidity for the acquisition of 1 set, QD is 4 times faster than STopo. Nevertheless, it is necessary to mention that the preparing time needed before the first QD set is still a higher than for STopo. This aspect can be and have to be improved in the future.

Table 4. Summary of the QDaedalus (QD) angular measurements on the dam.

Results	Zenith angles	Hz directions
# targets	18	18
# sets	3	3
Time for 1 set	3 min	3 min
Std dev. of 1 set	0.4 arcsec	0.4 arcsec
Std dev. mean	0.3 arcsec	0.2 arcsec

In order to evaluate the accuracy or the outer precision of the systems, we can compare the final angular values of QD with respect to STopo.

Table 5. Summary of the swisstopo semi-automatic (STopo) angular measurements on the dam.

Results	Zenith angles	Hz directions
# targets	18	18
# sets	2	2
Time for 1 set	12 min	12 min
Std dev. of 1 set	0.8 arcsec	1.0 arcsec
Std dev. mean	0.5 arcsec	0.7 arcsec

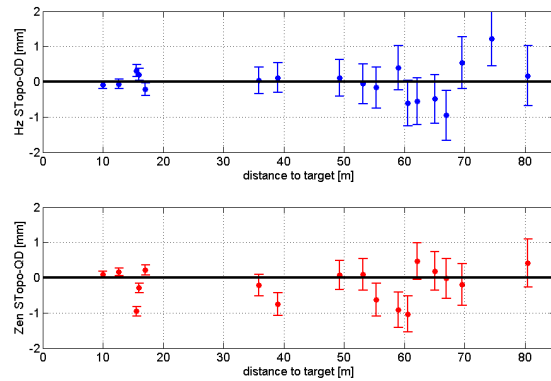


Fig. 6 Differences of the angular measurements (with 3-sigma confidence region) on the dam between QD and STopo.

The differences between QD and STopo for the horizontal directions and the zenithal angles are shown in Figure 6 in terms of lateral differences and summarized in Table 6. The error bars represent the empirical 3-sigma confidence regions of the differences between QD and STopo.

Table 6. Summary of the differences between the angular measurements carried out on the dam by swisstopo and the system QDaedalus.

Results	Zenith angles	Hz directions
Min	0.1 arcsec (0.0 mm)	0.2 arcsec (0.0 mm)
Max	12.6 arcsec (2.7 mm)	4.1 arcsec (1.2 mm)
Mean	1.5 arcsec (0.3 mm)	0.0 arcsec (0.1 mm)
Std dev	3.9 arcsec (0.8 mm)	2.0 arcsec (0.5 mm)

As we can see, the differences are in the sub-millimeter order of magnitude for all targets. Nevertheless, the results exhibit that the differences

are statistically significant for almost the half of the targets. This means that it exists some systematic errors between QD and STopo. With this set of data, it is difficult to quantify the amount of systematic errors which can be attributed to QD and/or STopo. Nevertheless, we can assert that the accuracy of the system QDaedalus is comprised between ~ 0.5 arcsec (0.15 mgon) and ~ 1.5 arcsec (0.5 mgon).

4 Dynamic 3D Deformation Monitoring of a Hybrid Structure with Hardwood

The study of the behaviour, the evolution and the health of existing structures by measuring responses to dynamic loads is nowadays a common task in civil or mechanical engineering. Usually, the responses are captured by accelerometers and/or displacement sensors fixed to the structure of interest. Depending on the modal characteristics which have to be determined, the sensors must fulfill some particular specifications. If only the natural frequencies are of interest, the sensors are chosen in function of their sensitivity, bandwidth and acquisition rate. If the determination of mode shapes is of interest, the quality of the synchronization and the 3D capabilities are also an essential issue. Concerning the choice of measuring rather accelerations than displacements or vice versa, the tendency is to prefer accelerations for the measurements of responses at high frequencies (> 1 Hz), and displacements for low frequencies responses (< 1 Hz). This is mainly due to the fact that the sensitivity of accelerometers are usually much higher than displacement sensors at high frequencies. Furthermore, apart from the cost, the choice of installing accelerometers rather than displacement sensors is also dictated by the fact that the setup of accelerometers is more convenient. In fact, they do not need to rely on external references as for displacement or positioning sensors. Nevertheless, regardless from noise aspects, displacements are conceptually more fundamental than accelerations. In fact the accelerations can be computed without loss of information from displacement data, while the displacements cannot be completely recovered by accelerations (two integration constants are ambiguous).

In this context, we try to deploy the system QDaedalus for the measurement of positions in 3D at high frequency (60 Hz). In previous experiments, Charalampous et al. (2014) showed that 2 synchronized QDaedalus systems were able to measure displacements at 60 Hz (in 2D, orthogonal

to the line of sight of the telescopes) of 2 LEDs attached on a rigid prototype with a sub-mm accuracy.

In this paper, the determination of 60 Hz sub-mm absolute 3D positions is investigated. For this purpose, 4 synchronised QDaedalus systems were pointing on 2 LEDs (D1 & D2) located on an innovative hybrid structure in hardwood designed by the Institute of structural engineering of ETH Zurich (Figure 7). In order to derive their modal characteristics the structure was excited by a shaker and monitored by 18 synchronized 3-axis MEMS accelerometers of type LIS344 with a sampling rate of 1kHz (Leyder et al. 2015). The LED D2 was located at almost the same position than the accelerometer A93 and allowed us to make some cross comparisons and validations between both measurement systems.

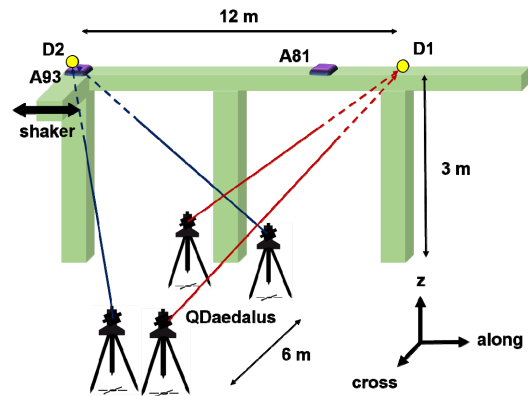


Fig. 7 Experimental setup placed on the hybrid wood structure.

4.1 QDaedalus Data Acquisition and 3D Adjustment

The raw observations consist, on the one hand, in a set of classical non-kinematic angular observations on the station observing the same LED, and on the other hand, in the time series of kinematic angular observations on the LEDs D1 and D2 (Figure 8). For each station, the kinematic observations are formed on the one hand by a 1 Hz time series of the angular readings of the total station, poorly synchronized through the clock of the computer, and on the other hand, by a 60 Hz time series of the center of mass of the LEDs on the CCD, perfectly synchronized on a hardware level, thanks to the synchronization boxes (Figure 3).

In a first preprocessing step, the angular readings of the total station are filtered and interpolated at the time of the CCD epochs. In a second preprocessing step, the angular readings and the CCD positions are combined according to Bürki et al. (2010) in order to get the horizontal direction and the zenith angle of the LEDs for all epochs.

Once all angular observations at all epochs are available, a 3D least-squares adjustment is performed. The mathematical model is simple and consists in considering all epochs in a single block. The observation equations for the horizontal direction r_{ij} and the zenith angle z_{ij} , between a station i and a target j (can be another station, or a LED at epoch t , $\mathbf{D}(t)$) are defined as follows:

$$r_{ij} + \hat{v}_{r_{ij}} = \arctan\left(\frac{\hat{y}_j - \hat{y}_i}{\hat{x}_j - \hat{x}_i}\right) - \hat{\omega}_{0i} \quad (1)$$

$$z_{ij} + \hat{v}_{z_{ij}} = \arctan\left(\frac{\sqrt{(\hat{y}_j - \hat{y}_i)^2 + (\hat{x}_j - \hat{x}_i)^2}}{\hat{z}_j - \hat{z}_i}\right)$$

where \hat{v} represents estimated residuals, $(\hat{y}, \hat{x}, \hat{z})$ the “cross”, “along” and “z” estimated coordinates according to Figure 7 and 8 and $\hat{\omega}_{0i}$ the orientation unknown of the station i . The stochastic model defines a constant standard deviation of 1 arcsec for all observations considered as uncorrelated. In addition, the model is augmented by the 5 following conditions:

$$d\hat{y}_{St1} = 0, d\hat{x}_{St1} = 0, d\hat{z}_{St1} = 0, \quad (2)$$

$$d\hat{y}_{St2} = 0, d\hat{x}_{St2} = 0$$

The \hat{z}_{St2} component is not constrained in because its estimation is much more accurate than its a priori known value.

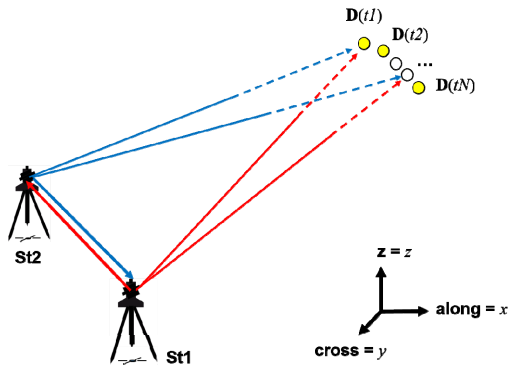


Fig. 8 Observations considered in the 3D adjustment processing.

For an acquisition time of 100 sec, the number of observations and unknowns are equal to $n=24'000$ and $u=18'000$, respectively. This generates large but sparse matrices which requires the use of a sparse matrix library.

4.2 Results of a Static Experiment

In order to quantify the noise of the systems, a static acquisition was carried out during 120 sec. The time series of the 3D positions of the LEDs D1 and D2 are shown in Figure 9. The Allan deviations of the 2 components of the LED D2 are shown in Figure 10. They show that the standard deviations are almost always below 0.01 mm for acquisition times below 1 minute.

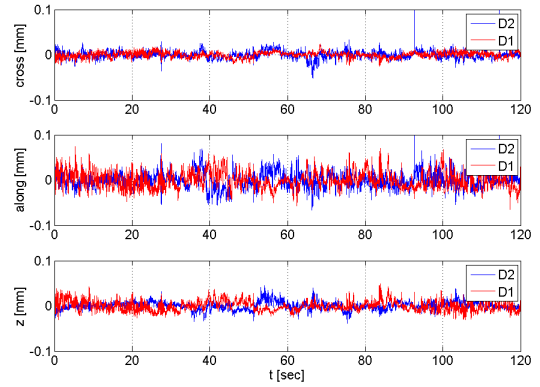


Fig. 9 Time series of the 3D coordinates of the LEDs in a static experiment.

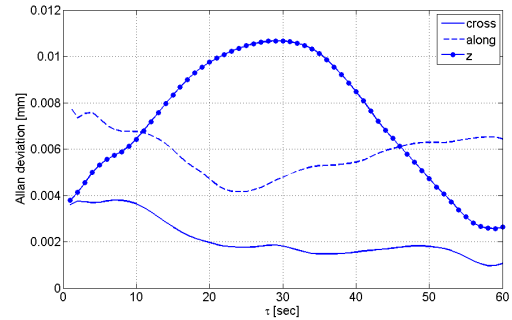


Fig. 10 Allan deviation of the times series of the LED D2 shown in Figure 9.

In order to compare the performance of QDaedalus with respect to the accelerometers used in this experiment, the amplitude spectrum of the displacements and accelerations of the LED D2 and the accelerometer A93 are shown in Figure 11 and 12. The QDaedalus accelerations are computed by a simple double numerical differentiation while the

accelerometer displacements $x_{acc}(t)$ are computed from the accelerations $a_{acc}(t)$ using the frequency dependent scaling in the frequency domain:

$$F\{x_{acc}(t)\} = X_{acc}(f) = \frac{1}{(i \cdot 2\pi \cdot f)^2} F\{a_{acc}(t)\} \quad (3)$$

$$x_{acc}(t) = F^{-1}\{X_{acc}(f)\}$$

where $F\{\}$ represents the Fourier transform operator.

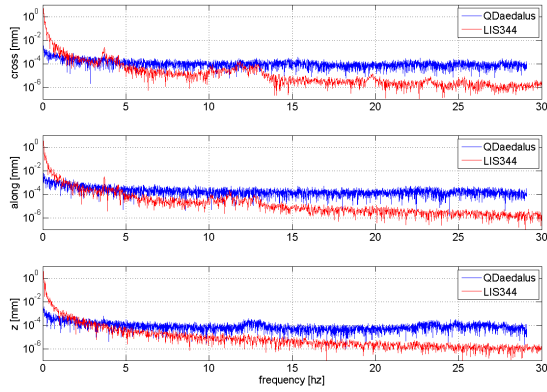


Fig. 11 Amplitude spectrum of the displacements from the QDaedalus and the accelerometer data.

The main outcome of the comparison of the spectra is that the QDaedalus system has a better sensitivity for measuring displacements and accelerations up to a frequency of approximately 3 Hz.

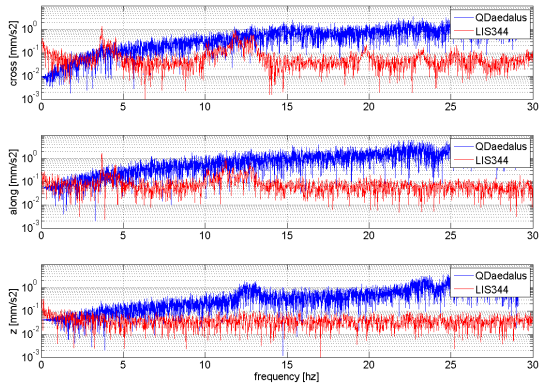


Fig. 12 Amplitude spectrum of the accelerations from the QDaedalus and the accelerometer data.

4.3 Results of a Dynamic Experiment

In a second experiment, the structure was excited with sine sweep from 10 to 17 and back to 10 Hz,

with a sweep velocity of 0.1 Hz/sec. The time series of the QDaedalus and accelerometer data are high-pass filtered at 1 Hz. The 3D positions of the LEDs D1 and D2 measured by the 4 QDaedalus systems are shown in Figure 13 and 14.

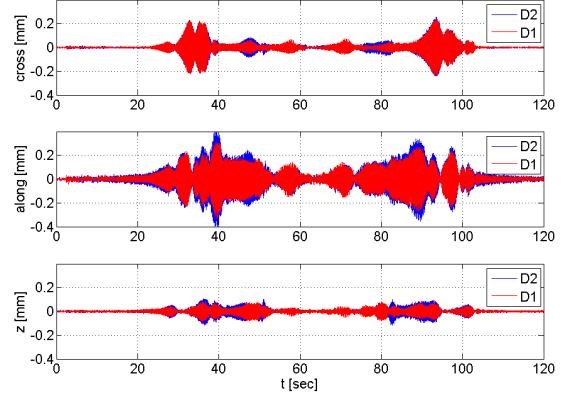


Fig. 13 QDaedalus 3D positions time series of D1 & D2.

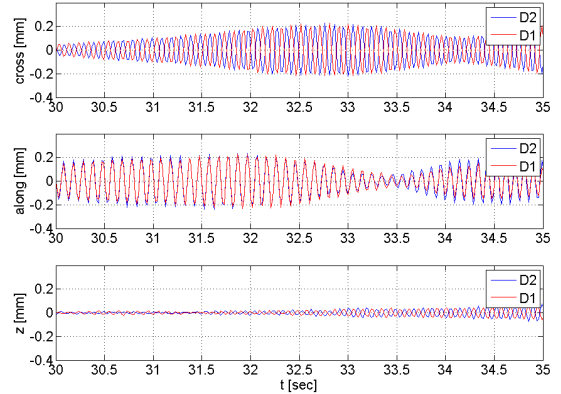


Fig. 14 Time series D1 & D2 of Fig. 13 (30 to 35 sec).

The time series show a very good agreement in amplitude between the 3D positions of D1 and D2. The 180 degrees phase difference in the cross and z directions can be easily explained from the modal characteristics of the structure. Here we can see that the synchronization of the QDaedalus systems is working properly.

In order to validate and cross check the data obtained by QDaedalus and the accelerometers, we can compare the time series of the displacements of the LED D2 to one obtained from the accelerometer A93. The time series are shown in Figure 15 and 16. In the shaking direction (along direction), the time series are very similar and reveal the resolution of both systems. Concerning the cross and the height components, the phases are also matching but we

can see that there are some significant differences in the amplitudes and in the shapes of the time series.

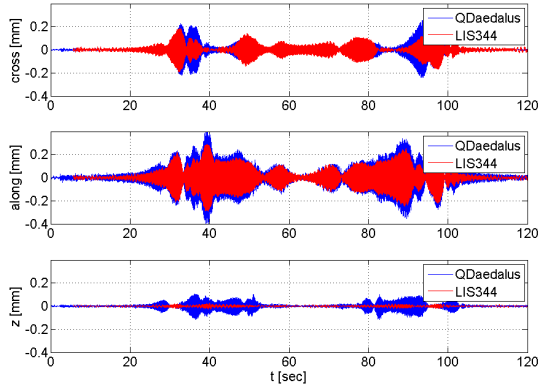


Fig. 15 Displacement time series of D2 & A93.

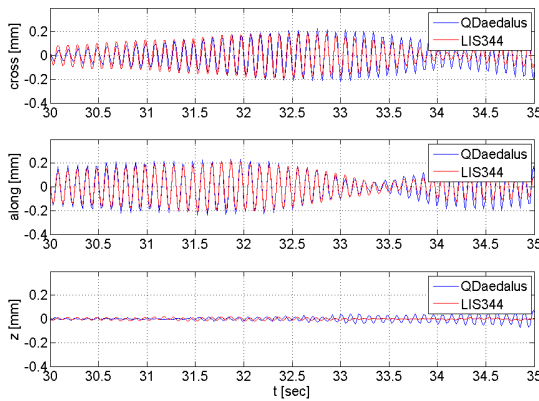


Fig. 16 Displacement time series of D2 & A93 (30-35 sec).

The differences are even clearer when we look at the amplitude spectra in Figure 17. Although the peaks are present at the same frequencies, the amplitudes differ significantly. In a first viewpoint, this can be mostly attributed to the fact that the LED D2 and the accelerometer A93 are not exactly collocated and not subjected to the same displacements on the cross and z axis. In fact, the A93 is placed on the neutral column axis while the LED D2 is located closer to the boundary of the column, and therefore more exposed to bending and torsional modes.

In order to investigate in more detail the precision of the QDaedalus system for 3D high frequency positioning, it is necessary to set up an experiment where an accelerometer is perfectly collocated with an optical target observed from 3 or more QDaedalus stations. With this significant redundancy, the quality of the 3D time series could be analysed in a more quantitative way.

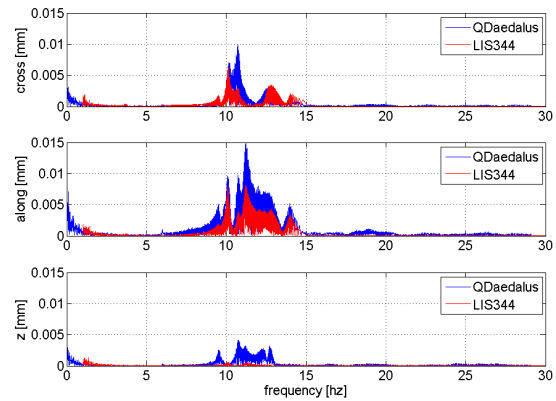


Fig. 17 Spectrum of the displacements of D2 and A93.

References

- Knobloch, S. (2009). Entwicklung, Kalibrierung und Erprobung eines kameraunterstützten Hängetachymeters, *Dissertation, Techn.Univ. Dresden*.
- Guillaume, S., Bürki, B., Griffet, S., Mainaud Durand, H. (2012). QDaedalus : Augmentation of Total Stations by CCD Sensor for Automated Contactless High-Precision Metrology, *FIG Working Week 2012, Rome, Italy*.
- Clerc, J. (2015). Automated Measurement of Passive Targets for Dam Monitoring using an Image-Assisted Theodolite. *Master Thesis, ETH Zürich*.
- Luhmann, T., Robson, S., Kyle, S., and Boehm, J. (2014). Close-Range Photogrammetry and 3D Imaging. *De Gruyter, 2nd edition edition*.
- Liao, P.-S., Chen, T.-S., and Chung, P.-C. (2001). A fast algorithm for multilevel thresholding. *Technical report, Department of Electrical Engineering, Cheng Shiu Institute of Technology, Kaohsiung, 833 Taiwan*.
- Canny, J. (1986). A Computational Approach to Edge Detection. *IEEE Trans. Pattern Analysis and Machine Intelligence*, 8(6):679–698, 1986.
- Fitzgibbon, A. W. and Fisher, R. B. (1995). A buyer's guide to conic fitting. *In Proc. of the British Machine Vision Conference*, pages 261-265.
- Charalampous, E., Psimoulis, P., Guillaume, S., Spiridonakos, M., Klis, R., Bürki, B., Rothacher, M., Chatzi, E., Luchsinger, R., Feltrin, G. (2014). Measuring sub-mm structural displacements using QDaedalus: a digital clip-on measuring system developed for total stations. *Applied Geomatics, Italian Society of Photogrammetry and Topography, Springer*.
- Leyder, C., Wanninger, F., Frangi, A., Chatzi, E. (2015). Dynamic response of an innovative hybrid structure in hardwood, *Proceedings of the Institution of Civil Engineers*.
- Bürki, B., Guillaume, S., Sorber, P., Oesch, H.-P. (2010). DAEDALUS: A versatile usable digital clip-on measuring system for Total Stations, *International Conference on Indoor Positioning and Indoor Navigation (IPIN)*, Zürich, IEEE.